CORA Cork Open Research Archive
Cartlann Taighde Oscailte Chorcaí

Title	Stability analysis of virtual power plant with grid forming converters
Authors	Tozak, Macit;Taskin, Sezai;Sengor, Ibrahim;Hayes, Barry P.
Publication date	2024-10-04
Original Citation	Tozak, M., Taskin, S., Sengor, I. and Hayes, B. P. (2024) 'Stability analysis of virtual power plant with grid forming converters', 2024 International Conference on Smart Energy Systems and Technologies (SEST), Torino, Italy, 10-12 September 2024, pp. 1-6. https://doi.org/10.1109/SEST61601.2024.10694439
Type of publication	Conference item
Link to publisher's version	10.1109/SEST61601.2024.10694439
Rights	© 2024, IEEE. Personal use of this material is permitted. Permission from IEEE must be obtained for all other uses, in any current or future media, including reprinting/republishing this material for advertising or promotional purposes, creating new collective works, for resale or redistribution to servers or lists, or reuse of any copyrighted component of this work in other works.
Download date	2026-11-03 00:02:49
Item downloaded from	https://hdl.handle.net/10468/16690



University College Cork, Ireland
Coláiste na hOllscoile Corcaigh

Stability Analysis of Virtual Power Plant with Grid Forming Converters

Macit Tozak
Dept. of Electrical - Electronics Engineering
Manisa Celal Bayar University
Manisa, Türkiye
macit.tozak@cbu.edu.tr

Sezai Taskin
Dept. of Electrical - Electronics Engineering
Manisa Celal Bayar University
Manisa, Türkiye
sezai.taskin@cbu.edu.tr

Ibrahim Sengor
Dept. of Electrical and Electronic Engineering
Munster Technological University
Cork, Ireland
ibrahim.sengor@mtu.ie

Barry P. Hayes[1,2]
[1]*School of Engineering,University College Cork*
[2]*MaREI the SFI Research Centre*
Cork, Ireland
barry.hayes@ucc.ie

***Abstract*—A virtual power plant is a system containing multiple distributed generators aggregated and flexibly coordinated to act as a single power source. This study investigates the active power, reactive power, frequency, and voltage support provided by a virtual power plant interconnected with the grid. The investigation encompasses the analysis of grid-forming (GFM)-controlled wind and solar power plant units, considering the fluctuating power generation from solar and wind sources. The real hourly wind and solar generation profiles from currently operational plants are used as the active power set points. The stability and power reference tracking of grid-connected converters are analyzed using dispatchable virtual oscillator control (dVOC) and droop control-based methods. The results show that both control strategies substantially improve the virtual power plant's ability to ensure grid stability and accurately track power references, despite the inherent variability of wind and solar energy generation.**

***Index Terms*—virtual power plant, grid-forming converter, dispatchable virtual oscillator control, droop control**

I. Introduction

Integrating renewable energy sources into the power grid is critical for sustainable energy systems. In line with the International Energy Agency (IEA) Net Zero Emissions by 2050 Scenario, by 2028, renewable energy sources will contribute to 42% of global electricity generation, with wind and solar photovoltaic (PV) collectively representing 25% of this share [1]. However, it also poses significant challenges regarding grid stability and reliability due to the reduction of system inertia [2], [3]. Maintaining grid stability becomes increasingly complex as the global energy paradigm shifts from centralized generation to more distributed energy resources (DERs) such as wind farms and PV plants. This complexity arises from renewable energy sources' intermittent and variable nature and requires advanced management and control strategies [4]. The Virtual Power Plant (VPP) concept is a promising solution to this challenge. This system combines the capacities of multiple distributed generators to act as a single reliable power source. VPP is a structure controlled to obtain collective behavior from mixed-type distributed generation units. A VPP should meet the demand according to an energy management strategy while providing ancillary services to the grid, such as voltage and frequency support [5].

In the literature, there are some studies on VPP regarding optimum operation [6], energy management [7], [8], and energy markets [9]. However, the number of studies on frequency and voltage stability by designing a suitable control scheme for VPP containing grid-forming (GFM) converters is quite limited. In [10], a reduced-order aggregated model was proposed to represent the VPP's transients and perform the system's transient stability analysis. In [11], an adjustable inertia support was provided by the synchronous VPP based on GFM inverter-interfaced distributed energy resources. In [12], [13], GFM and GFL control design approaches were proposed for dynamic VPPs to provide ancillary services such as fast frequency and voltage control. Experimental validation of a dynamic VPP controller on a power hardware-in-the-loop test bed was presented in [14]. In [15], coordinated and non-coordinated frequency control of VPPs with distributed generators on power system transients were investigated. Also, variations in wind-based power generation and voltage-dependent loads were taken into account. In [16], a coordinated frequency control strategy for VPPs composed of DERs was proposed to improve the short-term dynamic response of the overall power system. Reference [17] proposed a capability-coordinated frequency control scheme for a VPP including pumped storage hydropower, a wind power plant, and an energy storage system to support the frequency nadir and reduce the steady-state error of system frequency. However, none of them combine GFM converters with different control approaches such as droop and dVOC methods, and use real data obtained from PV and wind power plants. Combining different control approaches is important to evaluate the control interaction between different converter types.

This paper investigates the stable operation of a VPP

containing both a dVOC and a droop-controlled source in case of a coordinated change of power set points depending on the weather. Data obtained from real power plants are used to determine wind and PV power set values. It highlights the importance of incorporating GFM-controlled wind and PV units into a VPP framework to overcome the challenges arising from the variable nature of renewable energy production. Also, the study focuses on critical aspects of VPP operation such as active power, reactive power, frequency, and voltage support, especially when connected to the transmission grid. Although DERs are capable of providing ancillary services independently, aggregating them through a VPP framework allows for a coordinated approach to deliver these services.

The remainder of the study is organized as follows. Section II provides the methodology and system description. The mathematical model and control blocks of the system are given in Section III. Simulation results are presented in Section IV. Finally, the paper concludes in Section V.

II. Methodology – Problem Formulation and System Description

The voltage and frequency support of the VPP at the point of connection is analyzed using the simplified system configuration given in Fig. 1. The system includes two GFM-controlled sources consisting of a wind and a PV plant. Additionally, a collective load model representing all the loads in the network has been used. The grid side is represented by a large scale synchronous generator (SG).

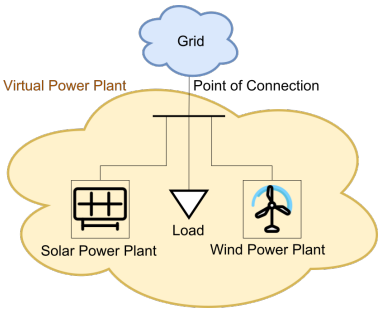


Fig. 1. Virtual power plant model connected to the grid.

Active power set points are determined using real hourly wind and PV generation profiles given in Fig. 2 on 8 May 2020 in İzmir and Manisa provinces of Türkiye. The active power set points are specified to be maximum generated hour is 1 p.u. and others are normalized according to the maximum point. The VPP controller instantly measures the active power values of all sources and loads. The controller determines power reference values according to weather changes and tries to ensure the power balance considering the currently available power of the system by keeping the frequency and voltage at nominal values.

The most common GFM control methods in the literature and practical applications are droop control and virtual synchronous generator (VSG) control [18]. However, there is a growing consensus that dispatchable virtual oscillator control (dVOC) is one of the valid GFM methods in terms of system

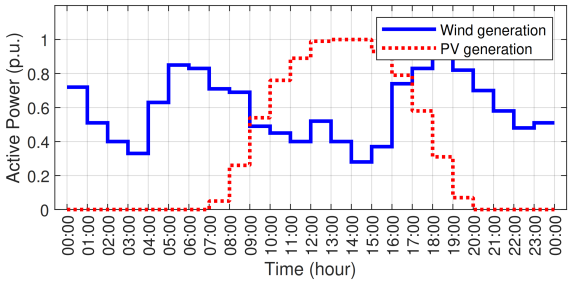


Fig. 2. Hourly normalized wind and PV generation profiles on 8 May 2020 in the İzmir-Manisa region, Türkiye.

TABLE I
System Parameters

Parameter	Symbol	Value
Base value	S_b	100 MVA
Base frequency	f_b	50 Hz
Base angular frequency	ω_b	2*pi*fb rad/sec
Base load		150 MW
Filter resistance	R_f	0.0005 pu
Filter capacitance	C_f	0.1885 pu
Filter inductance	L_f	0.0314 pu
Grid resistance	R_g	0.0055 pu
Grid inductance	L_g	0.1637 pu
Resistance for DC side losses	R_{dc}	1.2 ohm
Nominal DC voltage	V_{dc}^*	2.45 kV
DC voltage control gain	k_{dc}	1666.7
Outer loop voltage control gains	kp_v_ac, ki_v_ac	0.001, 0.5
Inner loop voltage control gains	k_{pv}, k_{iv}	0.52, 232.2
Inner loop current control gains	k_{pc}, k_{ic}	0.73889, 0.0059
Droop coefficient	D_p	ω_b*0.01/Sb
dVOC gains	η, α	0.0209, 66667

performance [19], [20]. So, the dVOC method is applied to the wind turbine with GFM control in order to generate reference voltage phasor and frequency. Andronow Hopf type oscillator is used in dVOC since it is the most suitable type for GFM inverter applications, as it can generate harmonic-free waveforms without compromising dynamic performance [19]. A voltage-controlled droop is a well-known GFM control method. So it is used as a GFM control method for PV power plant.

The system is perturbed by changing the voltage and frequency of the grid (infinite bus) and then the system support capabilities of the converters are observed. Also, voltage and frequency variations in the infinite bus, generation outages, and load disturbances are considered. This study uses the grid codes to asses the control design effectiveness. All inferences are obtained based on the test system simulated in MATLAB/Simulink.

III. Mathematical Model of the System

A. Overview of Electrical Circuit and Control of Converter

The electrical circuit diagram and the control blocks of three phase grid-connected converter are given in Fig. 3. Here R_f, L_f and C_f are resistance, inductance, and capacitance of the filter, respectively. R_g and L_g are grid side resistance and inductance including that of the transformer. C_{dc} is the DC bus capacitance, while R_{dc} represents the losses. System parameters are given in Table I

As for control blocks, they consist of two parts: system level and device level [21]. System level control, including GFM methods such as dVOC and droop control, provides voltage amplitude ($\|v_f^*\|$) and phase angle (θ_c) references for device level control as well as frequency (ω_c). There are two types of inputs: system-level control block set values and measured values. The signals belonging to set values are given in blue, the signals of measured values are given in red color, and the controllers' output signals are given in green color with dashed lines in Fig. 3. p_c^* represents the active power set values, which come from Fig. 2, q_c^* is the reactive power set point, ω_c^* is the frequency reference, and V_c^* is the voltage reference. p and q are the measured active and reactive powers after the filter, respectively. They are calculated by measuring dq voltage at the filter capacitance ($v_{f,dq}$) and current flowing through the grid impedance ($i_{g,dq}$). v_{dc} is the measured DC bus voltage while v_{dc}^* is the reference value for v_{dc}. Device level control includes inner synchronous reference frame (SRF) voltage control, current limitation, SRF current control and DC voltage control blocks. First, voltage reference signal ($v_{f,dq}^*$) coming from system level GFM control is applied the device level SRF voltage control. Then new current reference ($i_{f,dq}^*$) for current limiter and inner SRF current control blocks is obtained.

Electrical equations for the system are given in (1), (2) and (3). These equations represent the dynamics of $i_{f,dq}$, $v_{f,dq}$ and $i_{g,dq}$, respectively.

$$\begin{bmatrix} \frac{di_{f,d}}{dt} \\ \frac{di_{f,q}}{dt} \end{bmatrix} = \begin{bmatrix} \frac{v_{sw,d}}{L_f} - \frac{v_{f,d}}{L_f} - \frac{R_f}{L_f} i_{f,d} + \omega_c i_{f,q} \\ \frac{v_{sw,d}}{L_f} - \frac{v_{f,d}}{L_f} - \frac{R_f}{L_f} i_{f,q} - \omega_c i_{f,d} \end{bmatrix} \tag{1}$$

$$\begin{bmatrix} \frac{dv_{f,d}}{dt} \\ \frac{dv_{f,q}}{dt} \end{bmatrix} = \begin{bmatrix} \frac{i_{f,d}}{C_f} - \frac{i_{g,d}}{C_f} + \omega_c \cdot v_{f,q} \\ \frac{i_{f,q}}{C_f} - \frac{i_{g,q}}{C_f} - \omega_c \cdot v_{f,d} \end{bmatrix} \tag{2}$$

$$\begin{bmatrix} \frac{di_{g,d}}{dt} \\ \frac{di_{g,q}}{dt} \end{bmatrix} = \begin{bmatrix} \frac{v_{f,d}}{L_g} - \frac{v_{g,d}}{L_g} - \frac{R_g}{L_g} i_{g,d} + \omega_c i_{g,q} \\ \frac{v_{f,q}}{L_g} - \frac{v_g}{L_g} - \frac{R_g}{L_g} i_{g,q} - \omega_c i_{g,d} \end{bmatrix} \tag{3}$$

B. Control Blocks

The converter control blocks consist of two parts: system level and device level. At the system level, voltage phase, frequency, and phase angle values are obtained. These values are used for device-level control.

1) System Level Control: In system-level control, active and reactive power control, frequency control, and voltage control are performed. Droop control and dVOC methods are used for the system-level frequency control. Droop control equations are given in (4) and (5). D_p is droop coefficient and it is calculated in such a way that the power droop as the inverter's rating will cause 0.1 Hz frequency increase $(2\pi 0.5)/(S_b)$. S_b is chosen as 100 MVA for this system. Besides droop control, as reactive power controller to generate magnitude of voltage reference (6) is used. The dVOC method is implemented by using (7) and (8) as described in [22]. Here, η and α are positive control gains and $\eta = 2\pi 0.5 V_m^2/S_b$ and $\alpha = V_m^2/10$.

$$\dot{\theta} = \omega \tag{4}$$

$$\omega = \omega^* + D_p \left(p^* - p\right) \tag{5}$$

$$\begin{bmatrix} v_{c,d}^* \\ v_{c,q}^* \end{bmatrix} = \begin{bmatrix} V^* + k_q(q^* - q) \\ 0 \end{bmatrix} \tag{6}$$

$$\dot{\theta} = \omega^* + \eta \left(\frac{p^*}{V^{*2}} - \frac{p}{\left\| |v_{f,dq}^*| \right\|^2} \right) \tag{7}$$

$$\begin{aligned} \left\| v_{f,dq}^* \right\| = \eta \left(\frac{q^*}{V^{*2}} - \frac{q}{\left\| v_{f,dq}^* \right\|^2} \right) \left\| v_{f,dq}^* \right\| + \\ \eta \frac{\alpha}{V^{*2}} \left(V^{*2} - \left\| v_{f,dq}^* \right\|^2 \right) \left\| v_{f,dq}^* \right\| \end{aligned} \tag{8}$$

2) Device Level Control: In the device level control SRF inner voltage control, current limitation, SRF inner current control and DC voltage control blocks are used and modulation index is obtained.

SRF Voltage Control: A PI controller is used to implement SRF voltage control using equations (9) and (10) [23]. Hence, reference voltage and measured voltage are compared, and a new current reference is obtained for SRF current control and current limitation blocks. k_{pv} and k_{iv} are proportional and integral control gains of the PI-based voltage controller, respectively. k_{ffi} is the feed-forward gain factor that enables or disables i_g current measurement.

$$\begin{bmatrix} i_{f,d}^* \\ i_{f,q}^* \end{bmatrix} = \begin{bmatrix} k_{pv}\left(v_{f,d}^* - v_{f,d}\right) + k_{iv} x_{v,d} - \\ C_f.\omega_c.v_{f,q} + k_{ffi}.i_{g,d} \\ - \\ k_{pv}\left(v_{f,q}^* - v_{f,q}\right) + k_{iv} x_{v,q} + \\ C_f.\omega_c.v_{f,d} + k_{ffi}.i_{g,q} \end{bmatrix} \tag{9}$$

$$\begin{bmatrix} \frac{dx_{v,d}}{dt} \\ \frac{dx_{v,q}}{dt} \end{bmatrix} = \begin{bmatrix} v_{f,d}^* - v_{f,d} \\ v_{f,q}^* - v_{f,q} \end{bmatrix} \tag{10}$$

Current Limitation: The AC current needs to be limited so as not to exceed the AC current limit to prevent the converter from malfunctioning. As for (11), the magnitude of measured current on filter inductance is limited to i_f^{max}.

$$\bar{i}_{f,dq}^* = \begin{cases} i_{f,dq}^*, & \||i_{f,dq}\|| \le i_f^{max} \\ i_f^{max}, & \||i_{f,dq}\|| > i_f^{max} \end{cases} \tag{11}$$

SRF Current Control: Limited reference current is compared by measured current and new voltage reference for the voltage after the switching stage is obtained by using equations (12) and (13). k_{pc} and k_{ic} are proportional and integral control gains of the PI-based current controller, respectively. k_{ffv} is the feed-forward gain factor that enables or disables v_f voltage measurement.

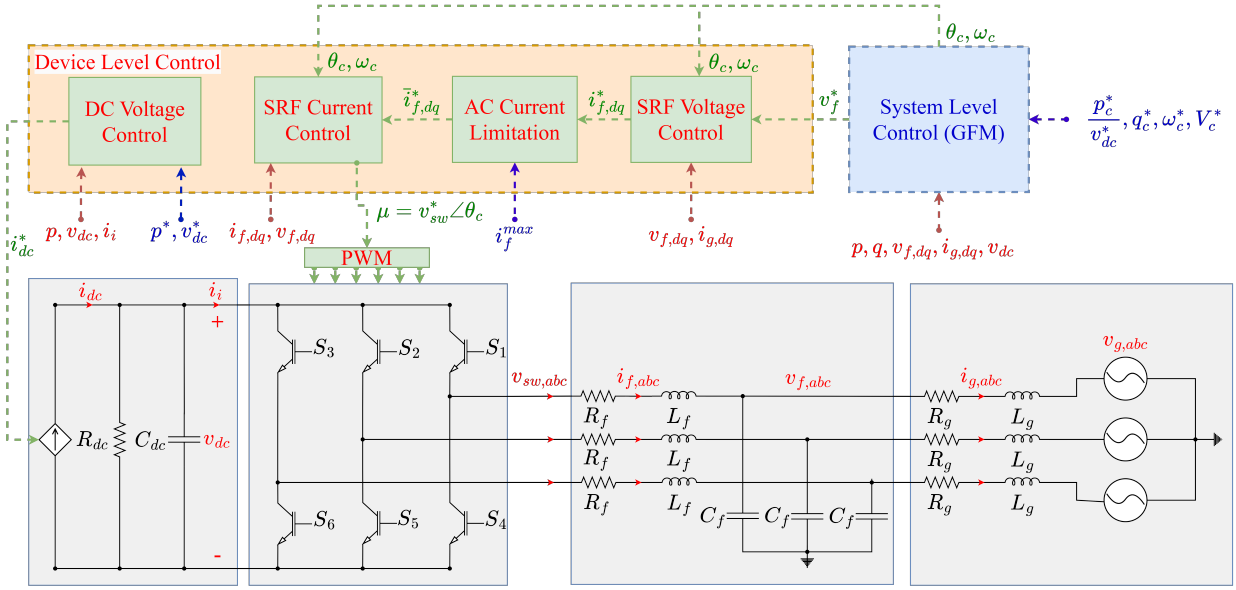


Fig. 3. Grid connected convertor configuration with control structure.

$$\begin{bmatrix} v^*_{sw,d} \\ v^*_{sw,q} \end{bmatrix} = \begin{bmatrix} k_{pc}\left(i^*_{f,d} - i_{f,d}\right) + k_{ic}.x_{i,d} \\ -L_f.\omega_c.i_{f,q} + k_{ffv}.v_{f,d} \\ - - - - - - - - - - - - - - - - - - \\ k_{pc}\left(i^*_{f,q} - i_{f,q}\right) + k_{ic}.x_{i,q} \\ +L_f.\omega_c.i_{f,d} + k_{ffv}.v_{f,q} \end{bmatrix} \tag{12}$$

$$\begin{bmatrix} \frac{dx_{i,d}}{dt} \\ \frac{dx_{i,q}}{dt} \end{bmatrix} = \begin{bmatrix} i^*_{f,d} - i_{f,d} \\ i^*_{f,q} - i_{f,q} \end{bmatrix} \tag{13}$$

Modulation Index: The modulation index (m_{abc}), which is used to get the PWM signal according to reference voltage ($v^*_{sw,abc}$) and DC voltage reference (v^*_{dc}) is obtained by (14). Here DC voltage reference is specified as $3V^*$.

$$m_{abc} = \frac{2v^*_{sw,abc}}{v^*_{dc}} \tag{14}$$

DC Voltage Control: DC current reference is obtained by (15) as given in [22]. In this process, the difference between the DC voltage measurement and DC voltage reference values is tried to be reduced. k_{dc} value is calculated as in (16). Also switching losses and converter DC losses are considered.

$$i^*_{dc} = k_{dc}\left(v^*_{dc} - v_{dc}\right) + \frac{p^*}{v^*_{dc}} + \left(\frac{v_{dc}}{R_{dc}} + \frac{v_{dc}i_i - p}{v^*_{dc}}\right) \tag{15}$$

$$k_{dc} = \frac{100S_b}{\left(v^*_{dc}\right)^2} \tag{16}$$

IV. Simulation Results

In this section, the simulation results of the system shown in Fig. 1 are given. The SG represents the grid. Wind and PV plants are included in the VPP and the effects of VOC and droop control on the variation of power set points are analyzed.

First, wind and PV power plants are both implemented by the dVOC method. The resulting active power and reactive power generations are given in Fig. 4, and frequency and voltage profiles are given in Fig. 5. In these figures, 98-124 seconds are zoomed in. Set values are drawn with dashed lines, while measured values are drawn with solid lines. Power set points are updated every 10.68 seconds according to the change in the weather-dependent wind and PV profiles given in Fig. 2. In Fig. 4a, it is seen that the sources share their power in accordance with the set values in approximately 6 seconds. In Fig. 4b, the change of reactive powers for each source is given. The reactive power setpoint for sources in VPP is set to 0. Frequency values at the connection point of all sources are shown in Fig. 5a, and voltage values are shown in Fig. 5b. After the events, the frequency settles at 1 pu within 6 seconds. It is seen that as the magnitude of the power changes increases, the amplitude of the spikes in the frequency and voltage measurements also increases.

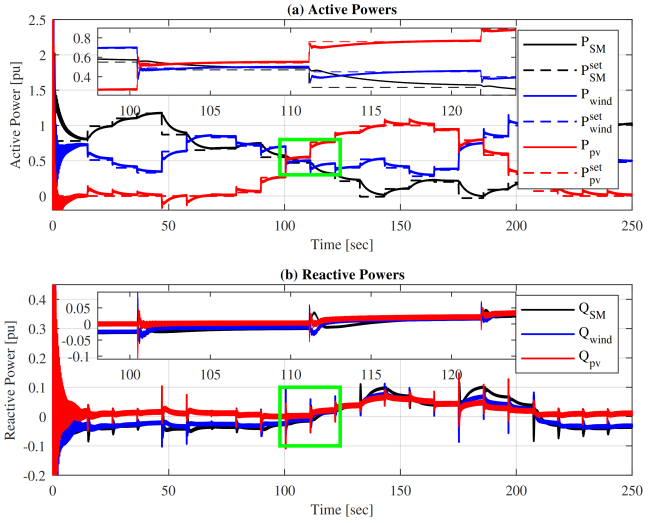


Fig. 4. The active and reactive power characteristic for dVOC based GFM controlled wind and PV generators connected to the grid.

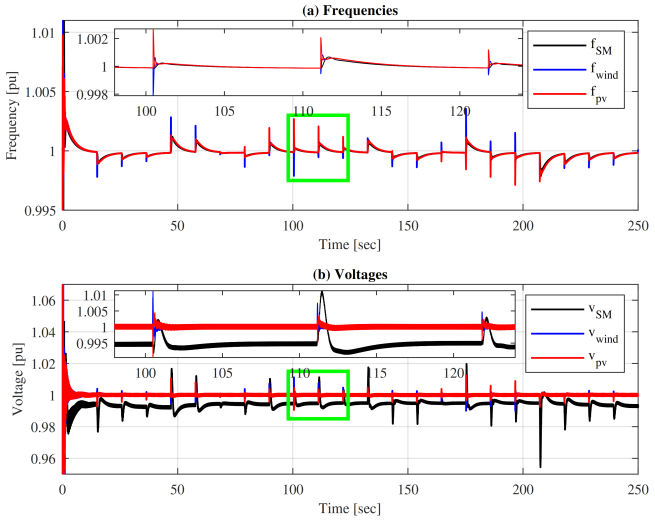


Fig. 5. The frequency and voltage characteristic for dVOC based GFM controlled wind and PV generators connected to the grid.

In a second scenario, the dVOC-controlled wind turbine and droop-controlled PV unit are connected to the grid. For each source, active and reactive power measurements are given in Fig. 6, and frequency and voltage measurements are given in Fig. 7. It is observed that the system response is similar when PV is controlled with droop control instead of dVOC. As the power set point changes in the VPP, the dynamic responses of the dVOC and droop control are similar and there is no negative control interaction that destabilizes the system.

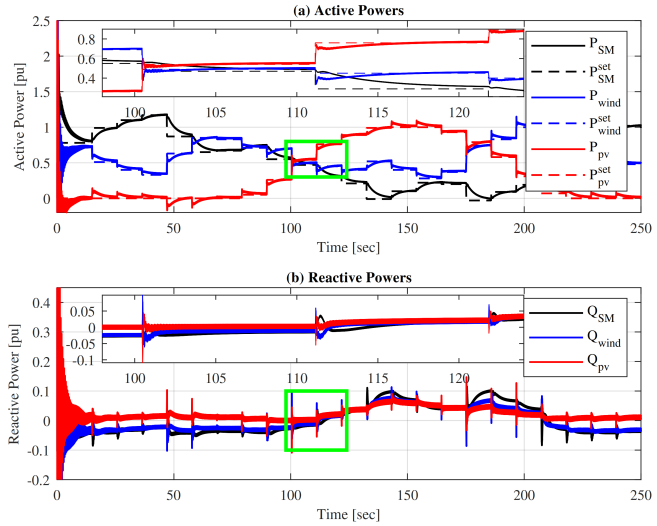


Fig. 6. The active and reactive power characteristic for dVOC-based GFM-controlled wind and droop-controlled PV connected to the grid.

The two cases are compared with numerical results regarding the active power, reactive power, frequency and voltage of the system as a result of the change in active power set values occurring in 111.14 seconds depending on weather conditions. Table II gives the measured and set values of active and reactive powers for two cases after the change of active power set values depending on weather conditions. Table III gives the measured frequency and voltages at each bus connected to sources after the active power set values

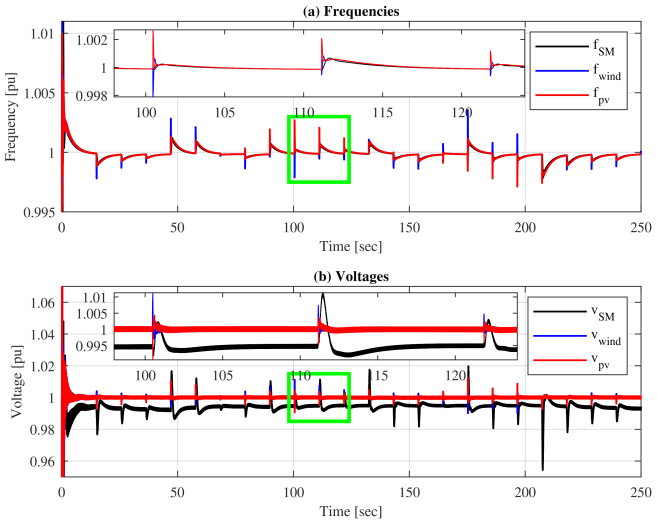


Fig. 7. The frequency and voltage characteristic for dVOC-based GFM-controlled wind and droop-controlled PV connected to the grid.

TABLE II
MEASURED AND SET VALUES OF ACTIVE AND REACTIVE POWERS FOR TWO CASES AFTER THE CHANGE OF ACTIVE POWER SET VALUES AT 111.14 SECONDS.

Cases	Power	Before Event		After Event	
		Set	Measured	Set	Measured
dVOC + dVOC	P_{SM}	0.47	0.488559	0.29	0.314755
	P_{wind}	0.49	0.503145	0.45	0.462999
	P_{pv}	0.54	0.55384	0.76	0.769108
	Q_{SM}	-	-0.0133467	-	0.0172729
	Q_{wind}	0	-0.0102965	0	0.0161569
	Q_{pv}	0	0.0024215	0	0.0203112
dVOC (wind) + Droop (pv)	P_{SM}	0.47	0.486216	0.29	0.315111
	P_{wind}	0.49	0.503473	0.45	0.462905
	P_{pv}	0.54	0.552492	0.76	0.768979
	Q_{SM}	-	-0.013978	-	0.0168618
	Q_{wind}	0	-0.0103468	0	0.0171596
	Q_{pv}	0	0.0024107	0	0.0232516

change. The average deviation between the two cases in active power measurements is calculated as 0.1563%, and in reactive power measurements, it is calculated as 4.7879%. The reason for the greater deviation in reactive power measurements is that the measured reactive power values are very small. When the frequency and voltage behaviors are examined for two cases, the obtained average deviation between; (i) steady-state frequency values is 0.0005%, (ii) steady-state voltage values is 0.059%, (iii) maximum frequency values are 0, (iv) maximum voltage values is 0.0155%, (v) the maximum % overhoot values of the frequency is 0.4717%, (vi) the maximum % overhoot values of the voltage is 12.0327 %. According to the results, the biggest difference between the two cases is obtained in the transient behavior of the voltages.

V. CONCLUSION

This study presented a comprehensive analysis of a VPP system, incorporating GFM-controlled wind and PV generation units, and its crucial role in providing stability, power reference tracking, active power, reactive power, frequency, and voltage support to the transmission grid. Through detailed simulations, leveraging real hourly wind and PV generation

TABLE III
MEASURED FREQUENCY AND VOLTAGES AT EACH BUS CONNECTED TO SOURCES FOR TWO CASES AFTER THE CHANGE OF ACTIVE POWER SET VALUES AT 111.14 SECONDS.

Cases	Measure-ments	f_{SM}	f_{wind}	f_{pv}	V_{SM}	V_{wind}	V_{pv}
dVOC + dVOC	Settling Value	0.9999	0.9999	0.9999	0.9953	1.0009	1.0009
	Max. Value	1.0007	1.0008	1.0021	1.0108	1.0075	1.0036
	Max. Over-shoot	0.0783	0.0917	0.2177	1.5544	0.6604	0.2697
dVOC (wind) + Droop (pv)	Settling Value	0.9999	0.9999	0.9999	0.9949	1,0002	1,0002
	Max. Value	1.0007	1.0008	1.0021	1.0110	1.0073	1.0035
	Max. Over-shoot	0.0788	0.0922	0.2182	1.6187	0.7167	0.3330

profiles from currently operating plants, we evaluated the performance of dVOC-based GFM control method alongside a hybrid approach combining dVOC and droop control.

In conclusion, this study contributed to the ongoing efforts to enhance the resilience, sustainability, and efficiency of power systems through the integration of renewable energy sources. It underscored the critical role of advanced control strategies in the operation of VPPs and their capacity to ensure stable and reliable grid performance in the face of fluctuating renewable energy outputs. The findings revealed that both control strategies, individually and together, in VPP controllers maintain grid stability and provide accurate power reference tracking in varying environmental conditions of wind and PV power generation.

Future research will focus on further refining these control strategies, exploring their scalability, and assessing their performance in larger, more complex grid environments to fully harness the potential of virtual power plants in the renewable energy landscape. Analyses based on eigenvalues will be performed to evaluate the stability limits of the system. A more realistic system including both GFM and GFL converters will be discussed. Experimental validation will also be carried out in the future.

REFERENCES

[1] Tech. Report, "Renewables 2023:Analysis and Forecast to 2028", International Energy Agency, Jan. 2024.

[2] R. H. Lasseter, Z. Chen, and D. Pattabiraman, "Grid-Forming Inverters: A Critical Asset for the Power Grid," IEEE J. Emerg. Sel. Top. Power Electron., vol. 8, no. 2, pp. 925–935, Jun. 2020.

[3] N. Modi, M. V. Escudero, K. Aramaki, X. Zhou, and P. Partinen, "High Inverter-Based Resource Integration: The Experience of Five System Operators," IEEE Power Energy Mag., vol. 22, no. 2, pp. 78–88, Mar. 2024.

[4] S. Anttila, J. S. Döhler, J. G. Oliveira, and C. Boström, "Grid Forming Inverters: A Review of the State of the Art of Key Elements for Microgrid Operation," Energies 2022, Vol. 15, Page 5517, vol. 15, no. 15, p. 5517, Jul. 2022.

[5] X. Wang, Z. Liu, H. Zhang, Y. Zhao, J. Shi, and H. Ding, "A Review on Virtual Power Plant Concept, Application and Challenges," 2019 IEEE PES Innov. Smart Grid Technol. Asia, ISGT 2019, pp. 4328–4333, May 2019.

[6] R. Heydari, J. Nikoukar, and M. Gandomkar, "Optimal Operation of Virtual Power Plant with Considering the Demand Response and Electric Vehicles," J. Electr. Eng. Technol., vol. 16, no. 5, pp. 2407–2419, Sep. 2021.

[7] M. M. Othman, Y. G. Hegazy, and A. Y. Abdelaziz, "Electrical energy management in unbalanced distribution networks using virtual power plant concept," Electr. Power Syst. Res., vol. 145, pp. 157–165, Apr. 2017.

[8] H. Ye, W. Pei, and Z. Qi, "Analytical modeling of inertial and droop responses from a wind farm for short-term frequency regulation in power systems," IEEE Trans. Power Syst., vol. 31, no. 5, pp. 3414–3423, Sep. 2016.

[9] S. R. Dabbagh and M. K. Sheikh-El-Eslami, "Risk Assessment of Virtual Power Plants Offering in Energy and Reserve Markets," IEEE Trans. Power Syst., vol. 31, no. 5, pp. 3572–3582, Sep. 2016.

[10] J. Chen, M. Liu, and F. Milano, "Aggregated Model of Virtual Power Plants for Transient Frequency and Voltage Stability Analysis," IEEE Trans. Power Syst., vol. 36, no. 5, pp. 4366–4375, Sep. 2021.

[11] Q. Hu et al., "Grid-Forming Inverter Enabled Virtual Power Plants with Inertia Support Capability," IEEE Trans. Smart Grid, vol. 13, no. 5, pp. 4134–4143, 2022.

[12] V. Häberle, A. Tayyebi, X. He, E. Prieto-Araujo, and F. Dörfler, "Grid-Forming and Spatially Distributed Control Design of Dynamic Virtual Power Plants," IEEE Trans. Smart Grid, pp. 1–1, 2023.

[13] V. Häberle, M. W. Fisher, E. Prieto-Araujo, and F. Dörfler, "Control Design of Dynamic Virtual Power Plants: An Adaptive Divide-and-Conquer Approach," IEEE Trans. Power Syst., vol. 37, no. 5, pp. 4040–4053, Sep. 2022.

[14] M. Andrejewski, V. Häberle, N. Goldschmidt, F. Dörfler, and H. Schulte, "Experimental validation of a dynamic virtual power plant control concept based on a multi-converter power hardware-in-the-loop test bench," pp. 697–704, Dec. 2023.

[15] W. Zhong, M. A. A. Murad, M. Liu, and F. Milano, "Impact of Virtual Power Plants on Power System Short-Term Transient Response," Electr. Power Syst. Res., vol. 189, p. 106609, Dec. 2020.

[16] W. Zhong, J. Chen, M. Liu, M. A. A. Murad, and F. Milano, "Coordinated Control of Virtual Power Plants to Improve Power System Short-Term Dynamics," Energies 2021, Vol. 14, Page 1182, vol. 14, no. 4, p. 1182, Feb. 2021.

[17] J. Kim et al., "Capability-coordinated frequency control scheme of a virtual power plant with renewable energy sources," IET Gener. Transm. Distrib., vol. 13, no. 16, pp. 3642–3648, Aug. 2019.

[18] D. Moutevelis, J. Roldán-Pérez, M. Prodanovic, and F. Milano, "Taxonomy of Power Converter Control Schemes based on the Complex Frequency Concept," IEEE Trans. Power Syst., vol. 39, no. 1, pp. 1996–2009, 2024.

[19] M. Lu, S. Dhople, and B. Johnson, "Benchmarking Nonlinear Oscillators for Grid-Forming Inverter Control," IEEE Trans. Power Electron., vol. 37, no. 9, pp. 10250–10266, Sep. 2022.

[20] X. He, V. Häberle, S. Member, F. Dörfler, and S. Member, "Complex-Frequency Synchronization of Converter-Based Power Systems," 2022.

[21] U. Markovic, "Towards reliable operation of converter-dominated power systems: Dynamics, optimization and control," ETH Zurich, 2020.

[22] A. Tayyebi, D. Gross, A. Anta, F. Kupzog, and F. Dorfler, "Frequency Stability of Synchronous Machines and Grid-Forming Power Converters," IEEE J. Emerg. Sel. Top. Power Electron., vol. 8, no. 2, pp. 1004–1018, Jun. 2020.

[23] S. D'Arco, J. A. Suul, and O. B. Fosso, "Control system tuning and stability analysis of Virtual Synchronous Machines," 2013 IEEE Energy Convers. Congr. Expo. ECCE 2013, pp. 2664–2671, 2013.